Anisotropic, three-dimensional deformation of single attached cells under compression

Annals of Biomedical Engineering, Vol. 32, No. 10, October 2004 (© 2004) pp. 1443–1452

Anisotropic, Three-Dimensional Deformation of Single Attached Cells under Compression

EMIEL A. G. PEETERS,[1,4] CARLIJN V. C. BOUTEN,[1] CEES W. J. OOMENS,[1] DAN L. BADER,[1,2] LUC H. E. H. SNOECKX,[1,3] and FRANK P. T. BAAIJENS[1]

[1]Department of Biomedical Engineering, Eindhoven University of Technology, Eindhoven, The Netherlands; [2]IRC in Biomedical Materials and Medical Engineering Division, Queen Mary, University of London, London, United Kingdom; and [3]Department of Physiology, Maastricht University, Maastricht, The Netherlands

(Received 26 March 2004; accepted 23 June 2004)

Abstract—Quantifying three-dimensional deformation of cells under mechanical load is relevant when studying cell deformation in relation to cellular functioning. Because most cells are anchorage dependent for normal functioning, it is desired to study cells in their attached configuration. This study reports new three-dimensional morphometric measurements of cell deformation during stepwise compression experiments with a recently developed cell loading device. The device allows global, unconfined compression of individual, attached cells under optimal environmental conditions. Three-dimensional images of fluorescently stained myoblasts were recorded with confocal microscopy and analyzed with image restoration and three-dimensional image reconstruction software to quantify cell deformation. In response to compression, cell width, cross-sectional area, and surface area increased significantly with applied strain, whereas cell volume remained constant. Interestingly, the cell and the nucleus deformed perpendicular to the direction of actin filaments present along the long axis of the cell. This strongly suggests that this anisotropic deformation can be attributed to the preferred orientation of actin filaments. A shape factor was introduced to quantify the global shape of attached cells. The increase of this factor during compression reflected the anisotropic deformation of the cell.

Keywords—Cell mechanics, Image analysis, Cell deformation, Muscle cell, Confocal microscopy.

INTRODUCTION

Many cells in mammalian organisms are permanently exposed to deformation. Cells are deformed by mechanical forces exerted by the external environment of the cell or generated by the internal cellular environment; a process that involves the conversion of chemical energy into mechanical energy.

The degree of cell deformation largely depends on the integrated internal structure of the cell and the connection of the cell to the external environment.[18,35] Internal structures, including the cell nucleus, cytoplasm, cytoskeleton, membranes, and organelles, provide resistance to deformation. Alterations in one of those structures can lead to an increased or decreased resistance to deformation. Likewise, cell–cell and cell–matrix interactions also affect cell deformability.[39] For example, spreading of specific cell types causes an increased mechanical resistance to deformation, presumably due to structural reorganization of the cytoskeleton during this process.[11,34]

Deformation of cells is believed to influence their biochemistry, function, and structure.[40] To study the effects of cell deformation, several experimental techniques are available, applying deformations to either specific parts of the cell (local deformation) or to the cell as a whole (global deformation). Local deformation experiments include partial micropipette aspiration,[31] cell poking,[12] atomic force microscopy,[1] and magnetic bead cytometry.[38] Global deformation experiments include the use of microplates,[35] micromanipulation,[43] cytoindentation,[23] and complete micropipette aspiration.[28]

The majority of these studies assume the shape of the cell to be spherical, axisymmetric or just consider a two-dimensional cross-section of the cell. Consequently, cell deformation is assumed to be isotropic and quantified from alterations in cell volume, surface area, or shape factors, such as the ratio of cell diameters.[16,22] Although these assumptions are valid for nonadherent cells, they are not appropriate for attached cells that are dependent on anchorage for normal functioning.[5] For example, many cell types that are allowed to spread, undergo growth and differentiation, whereas if they were constrained in a spherical form in culture, they would undergo either apoptosis or dedifferentiation.[10,27] *In vivo* and *in vitro* most cells are spread, attaching to either the extracellular matrix or the culture substrate. Therefore, it is physiologically relevant to study the deformation of attached cells. Because these cells show a more irregular shape than cells in suspension,

Address Correspondence to E. A. G. Peeters, Department of Biomedical Engineering, Eindhoven University of Technology, P.O. Box 513, Building W-hoog 4.123, 5600 MB Eindhoven, The Netherlands. Electroniv mail: e.a.g.peeters@tue.nl

it is desirable to obtain three-dimensional images of the cell during deformation experiments.

Confocal laser scanning microscopy provides a way to obtain three-dimensional images of living cells by making optical sections through the depth of the cell.[13,41] This technique has been successfully applied to study the deformation of chondrocytes and nuclei in articular cartilage explants.[15] However, the deformation of attached cells has never been investigated in three dimensions.

The present study aimed at quantifying the three-dimensional deformation of single cells in their attached configuration. Single C2C12 mouse myoblasts attached to a culture substrate were deformed using a specially designed loading device for unconfined compression under optimal environmental conditions, comparable to those of a regular CO_2 incubator.[29] The width, height, cross-sectional area, surface area, and volume of the cell during compression were estimated by means of combining confocal laser scanning microscopy with custom developed processing software. To quantify cell shape, a shape factor was introduced, which describes the ratio of the two major principal axes of the attached cell.

MATERIALS AND METHODS

Cell Culture

The C2C12 mouse skeletal myoblast line (ECACC, Porton Down, UK) was used in this study. The myoblasts were cultured in growth medium consisting of Dulbecco's modified Eagle medium supplemented with 15% fetal calf serum, 1% nonessential amino acid solution, 20 mM HEPES and 0.5% gentamicine (all from Biochrom AG, Berlin, Germany). Cells were used at passages 10–14.

Cell Loading Device

Cells were compressed with a single cell loading device, which is shown in Fig. 1 and described in detail elsewhere.[29] To review briefly, the device consists of a stainless steel frame resting on a motorized stage of an inverted microscope (Axiovert 100M, Zeiss, Göttingen, Germany) with a confocal laser scanning unit (LSM 510, Zeiss, Göttingen, Germany). Cells were grown on a cover glass, which was inserted in the cell chamber (3-mm deep and 25-mm diameter) of the frame. Within the cell chamber of the device, the temperature (37 °C) and the level of CO_2 (5%) were controlled as to provide physiological culture conditions.

To compress a single cell, a glass indenter (0.48-mm diameter) having a flat surface with a diameter of 60 μm (Fig. 1, inset) was used. The indenter was attached to a force transducer (model 406A, Aurora Scientific Inc., Ontario, Canada), which has a full scale range of 500 μN and a resolution of 10 nN. Forces imposed on the cell were measured and sampled, after a ten fold amplification, by a data-acquisition board (PCI-6052E, National Instruments,

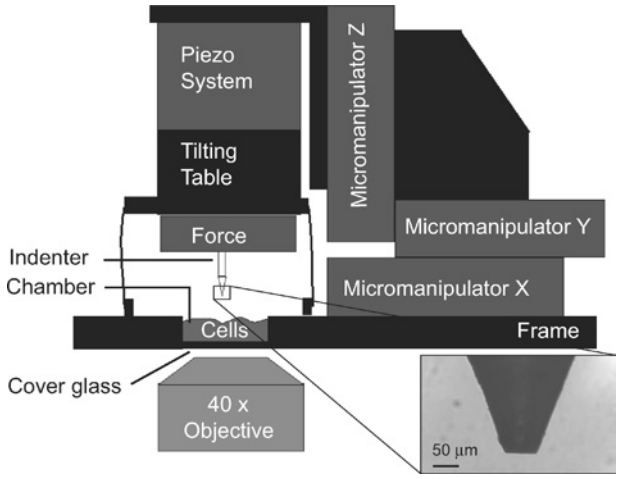

FIGURE 1. Schematic representation of the single cell loading device. The insert shows a close-up of the glass indenter.

Austin, TX). Using a tilting table, the force transducer could be twisted around two axes in the horizontal plane at a maximum of 2°. This ensures that the surface of the glass indenter was parallel with respect to the cover glass. The indenter was moved using three wide range (15 mm), low accuracy (100 nm) micromanipulators (M-111.DG, Physik Instrumente, Karlsruhe, Germany) and a small range (100 μm), high accuracy (5 nm) nanopositioning system with three piezo-actuators (Nanocube P-611, Physik Instrumente, Karlsruhe, Germany). The position of the micromanipulators and the piezo-actuators were controlled and recorded using a motor controller PC board (C-842, Physik Instrumente, Karlsruhe, Germany) and the data-acquisition board in a personal computer. Calibration of the piezo-actuators was carefully performed by the manufacturer and resulted in a displacement sensor sensitivity of 10 μm/V. Calibration of the force transducer was carried out by applying known weights to the hollow output tube of the transducer, resulting in a sensitivity of 5 μN/V. Compliance of the transducer was determined by compressing the indenter on a hard surface while simultaneously recording the position of the piezo-actuator and the force. This resulted in a compliance of 15 μm/mN.

Experimental Procedure

One day prior to the experiments, cells were seeded at subconfluent densities (10,000 cells/cm^2) on the cover glass within the stainless steel frame of the loading device. After allowing them to attach overnight, the cells were stained with 7.5 μM Cell Tracker Green (CTG, Molecular Probes, Leiden, the Netherlands), which stains the cytoplasm of the cells. Then, a cell was selected for compression and a complete stack of confocal images of the undeformed cell was recorded. The height of the cell was estimated using the imaging software of the microscope and the indenter was

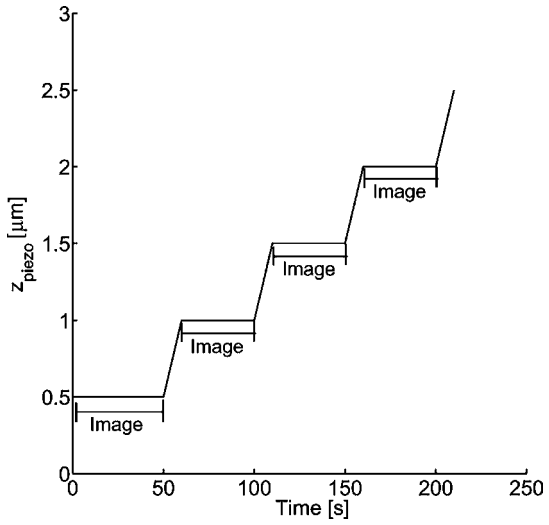

FIGURE 2. Schematic diagram of the loading protocol in which individual cells were compressed using compression increments of 0.5 μN. A complete stack of confocal images of the cell was recorded between two compression increments.

subsequently moved to the top of the cell. During the compression experiment, the indenter was lowered by 0.5 μm increments of axial displacement, followed by the recording of a stack of confocal images to visualize the complete deformed cell (Fig. 2). The position of the piezo-actuators and the force were recorded continuously. The experiment was ended when the output of the force transducer reached its maximal value of 50 μN. In total, 14 cells were subjected to the compression test protocols.

For confocal imaging, the cell was visualized using a 40×, air, 0.95 numerical aperture objective (Plan-Apochromat, Zeiss, Göttingen, Germany). The CTG stain was excited using the Argon ion laser at 488 nm. To compensate for geometric distortion due to a mismatch in refractive index of the immersion medium (growth medium) and the objective medium (air), a linear z-correction factor of 1.33 was introduced.[8,17,37] Images were recorded with a pixel size of 0.22 × 0.22 μm^2 and a slice thickness of 0.4 μm. After the experiment, the confocal images were deconvolved using the Huygens System image restoration software (Scientific Volume Imaging BV, Hilversum, the Netherlands). A theoretical point spread function was calculated using electromagnetic diffraction theory, while deconvolution was carried out by a maximum likelihood based algorithm.[21]

Data Analysis

Each stack of confocal images was analyzed with the aid of a custom software program in Matlab (The Mathworks, Natick, MA). All images were smoothed by a 2D median filter. To define the cell boundary, the images were thresholded using a full width half maximum threshold as adopted in previous studies.[6,22,24] The cell volume (V) was calculated by summing all relevant voxels and multiplying them by the voxel size. Relevant voxels were defined as those with a value of 1 and thus considered to be part of the cell. A three-dimensional reconstruction of the cell was created using the iso-surface method as implemented in Matlab. This routine forms a triangulation of the volume set and represents the object as a series of linked triangles. The surface area of the cell (SA) was then calculated by summing the areas of all triangles. The height of the cell (H) was calculated as an average of the height in a user-defined area at the top of the cell. For each point in this area, all voxels in the axial plane were summed and multiplied with the axial sampling distance. Assuming the density of the cell to be constant, the center of mass of the cell was determined by averaging the x, y, and z coordinates of all relevant voxels. The mass moments of inertia matrix of the cell at each compression step was determined with respect to a translated cartesian coordinate system with its origin located at the center of mass of the cell. Solving an eigenvalue problem, the orientation of the three principal axes of inertia was determined. These axes represent the three axes of an ellipsoid, which best matches the shape of the cell. The magnitude of each axis of the ellipse is given by

$$I_i = \frac{1}{\sqrt{\lambda_i}}, \tag{1}$$

in which λ_i is the eigenvalue of the eigenvector representing the corresponding principal axis. Now, a shape factor κ_{21} was defined as being the ratio between the magnitudes of the two major principal axes:

$$\kappa_{21} = \frac{I_2}{I_1}. \tag{2}$$

This shape factor is a unitless ratio that equals unity for a circle and diverges from unity for any other shape. It provides a measure to indicate the degree of deviation of a shape from circular (Fig. 3).

The width (W) of the cell was determined along the second principal axis of the cell. The cross-sectional area (A) of a slice through the center of mass of the cell was calculated by summing all relevant pixels and then multiplying this value by the pixel area. All geometric parameters obtained for each cell are summarized in Fig. 4.

To assess the accuracy of the method, the analysis was performed on two mathematically defined shapes and on images obtained from measurements on fluorescent beads with known diameter. The measured geometric parameters appeared to deviate less than 7% from their theoretically determined values (Appendix).

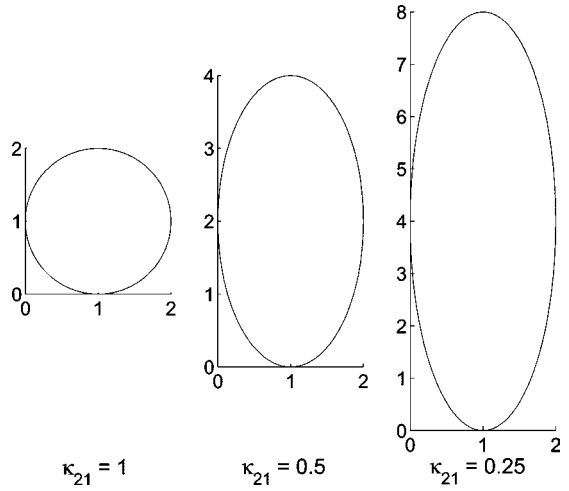

FIGURE 3. Shape factor κ_{21} describes the ratio between the magnitude of the first and the second principal axis. The values for κ_{21} are shown for three basic shapes.

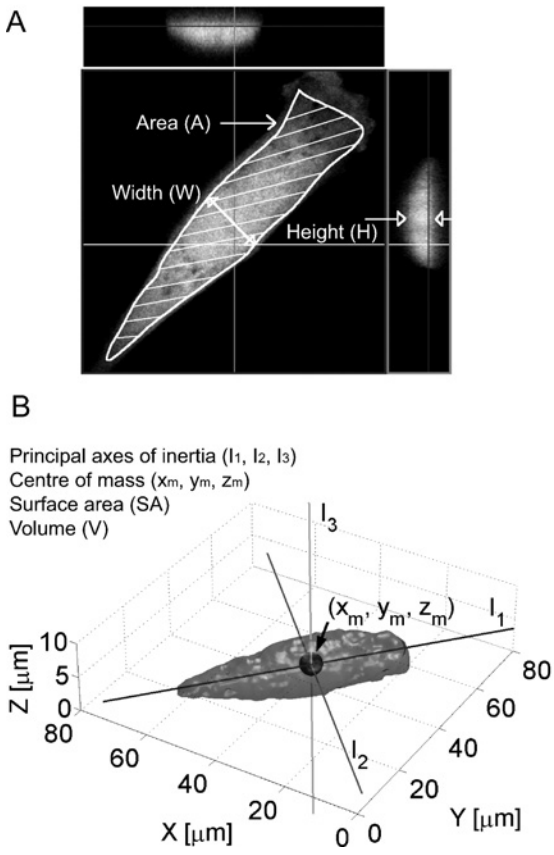

FIGURE 4. Overview of the geometric parameters obtained for each cell. An orthogonal projection of the cell (A) as well as a three-dimensional reconstruction (B) of the same cell are shown.

RESULTS

Orthogonal projections of a cell as recorded with confocal microscopy at six compression increments are shown in Fig. 5. From these typical images, flattening of the cell due to compression can be observed. The final image [Fig. 5 (F)] shows the cell when the cell membrane has been totally ruptured and only a thin layer of cell debris was left over. From these images two major phenomena can be observed. First, it can be seen that the cell deforms more in the direction of the second principal axis (I_2) than the first principal axis (I_1). This phenomenon was observed in all compression experiments.

In addition, the nucleus of the cell also deforms more in the direction of the second principal axis than of the first principal axis. In Fig. 5(A) the nucleus has an elliptical shape, whereas in Fig. 5(E), the nucleus adopts a more circular shape. This phenomenon was observed in all compression experiments when the nucleus was visible, which was the case in 70% of the experiments.

Deconvolution was applied to all confocal images. The effect of deconvolution was especially significant in the axial plane (XZ and YZ plane) of the images, which is shown in Fig. 6.

The initial values of the measured geometric parameters of all 14 cells in the undeformed situation are given in Table 1. In order to summarize the compression data, the changes as a percentage of the initial values for all geometric parameters and the shape factor were averaged for all cells and plotted against axial compression intervals of 10%. Only the data up to 50% axial deformation were taken into account, for at larger axial deformations the cells showed structural damage. The results of original and deconvolved images of compression experiments performed on the 14 cells are shown in Figs. 7 and 8. At each compression interval of 10%, difference from zero deformation for all geometric parameters and the shape factor was tested for statistical significance using a Student's t-test with a 0.05 level of significance. Cell width, area, and surface area all increased as a result of compression. There was also a slight increase in volume observed, although the volume increase was only statistically different from zero for the original images at the axial deformation of 45% [Fig. 7(D)]. After deconvolution, however, the volume increase was not statistically different from zero. The shape factor κ_{21} increased as a result of compression, implying that the cells deformed anisotropically from an elliptical to a more circular shape. The percentage change of κ_{21} was statistically significant from zero for each 10% increase in deformation up to 45% [Fig. 8 (B)].

DISCUSSION

In this study, the three-dimensional deformation of attached cells under compression was investigated and quantified using the width, area, surface area, and volume of the cell. In order to quantify cell shape and possible anisotropic

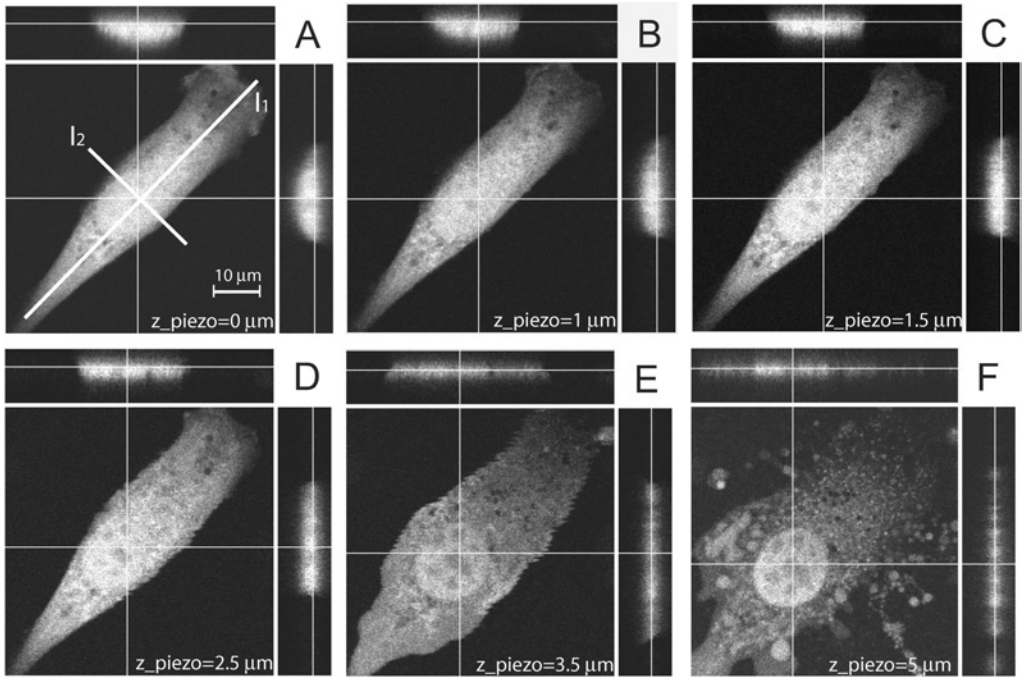

FIGURE 5. Orthogonal projections of a cell at six different compression increments obtained by confocal microscopy. (A) Shows the two major principal axes of the cell: I_1 and I_2. (F) Shows the cell when the maximum measurable force of the transducer was reached and only a thin layer of cell debris was left over. The ruptured membrane can be clearly seen.

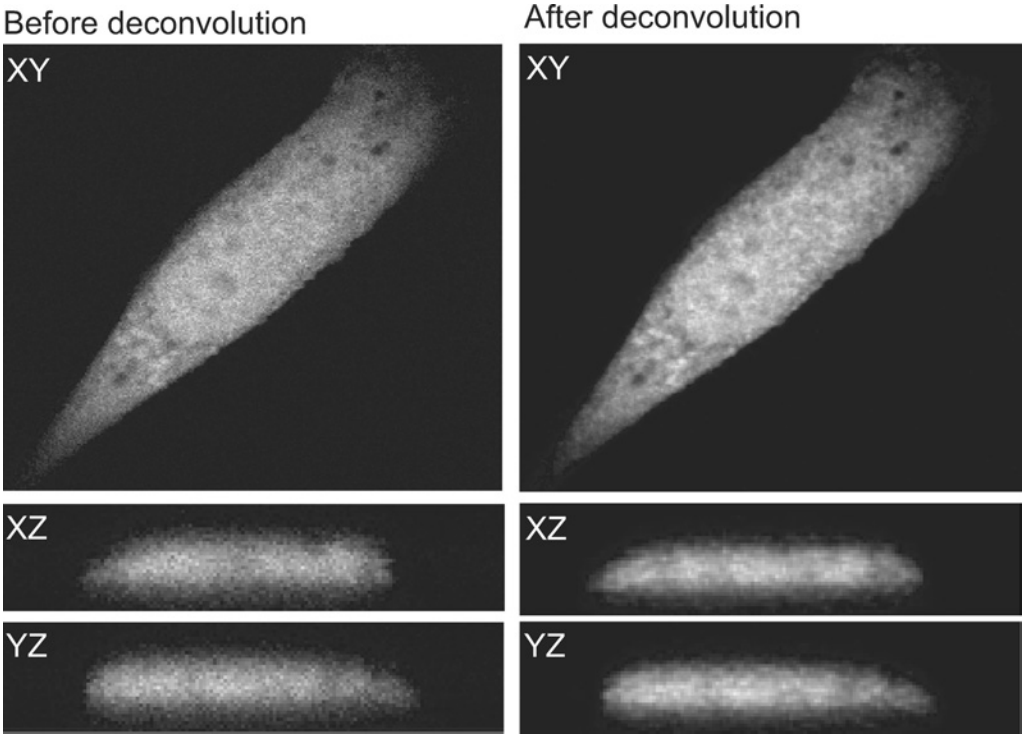

FIGURE 6. XY, XZ, and YZ plane of a stack of confocal images, before and after deconvolution.

TABLE 1. Initial values of width, height, area, surface area, and volume of 14 cells before a compression experiment was conducted (mean ± SD).

Width (μm)	Height (μm)	Area (μm^2)	Surface area (μm^2)	Volume (μm^3)
15.7 ± 2.0	6.7 ± 1.1	511 ± 140	1470 ± 380	2505 ± 710

deformations, a shape factor was calculated, describing the ratio between the two major principal axes of the cell. The use of confocal imaging and associated software allowed the three-dimensional quantification of cell deformation. Such a procedure obviated the need to make assumptions regarding the geometry of the cell.

Cells were allowed to attach and spread for at least 16 h. In contrast, other studies examining cell deformation using confocal microscopy investigated nonattached C2C12 myoblasts and chondrocytes, which have a more or less spherical morphology.[6,24] The large diameter of the indenter permitted the compression of the entire cell and not a part of the cell as in the case with other indentation techniques, such as atomic force microscopy[36,42] or cell poking.[26,30] Micropipette aspiration experiments also allow the deformation of the entire cell but are often only applied to suspended cells.[14,28] Cells can be deformed entirely using microplate manipulation,[35] but this technique allows the cell to attach for a maximum of 4 h, which is insufficient for C2C12 myoblasts to fully spread. Indeed, extended incubation times for cell attachment caused migration of the cell toward the edge of the microplate.[9]

The shape factor used in this study describes the shape of an ellipse, which best matches the shape of the cell. Although the use of the shape factor is comparable to the deformation index used in other studies[6,15,22] and to the shape factor used to describe cell reshaping in epithelia,[7] it has considerable advantages over those previously reported. First, the derivation of the shape factor through calculation of the principal axes of inertia is a relatively straightforward automatic method and thus free of operator error. A deformation index will be difficult to define for attached cells with their irregular shapes. Secondly, the shape factor describes the overall shape of the cell, which makes this method suitable to describe shape changes on a global cell level and to compare the deformation behavior of several cells.[7] In addition, the shape factor is based on the two major principal axes of the cell and independent of the orientation of the cell on the cover glass.

Cell width, area, and surface area increased during compression (Fig. 7). The increase of surface area is an apparent increase in the overall surface area, as the folds and ruffles in the cell membrane cannot be observed with confocal microscopy.[24] Furthermore, it should be noted that local membrane strains can be much larger than the overall measured membrane strain because the cells were able to

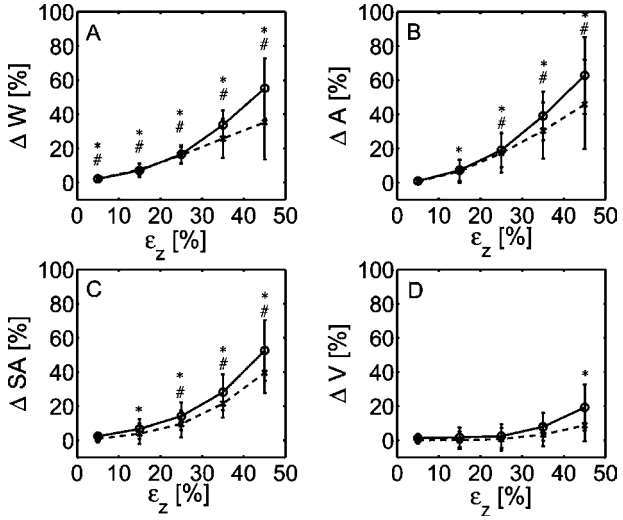

FIGURE 7. Average percentage changes of cell width (A), area (B), surface area (C), and volume (D) as a function of the axial deformation for 14 cells (mean ± SD) before (solid) and after (dashed) deconvolution. *Parameter differs significantly from zero, before deconvolution ($p < 0.05$). #Parameter differs significantly from zero, after deconvolution ($p < 0.05$).

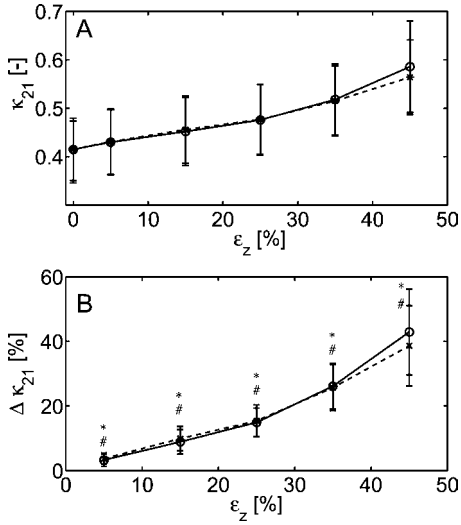

FIGURE 8. Average value (A) and percentage change of shape factor κ_{21} (B) as a function of the axial deformation for 14 cells (mean ± SD) before (solid) and after (dashed) deconvolution. *Parameter differs significantly from zero, before deconvolution ($p < 0.05$). Parameter differs significantly from zero, after deconvolution ($p < 0.05$).

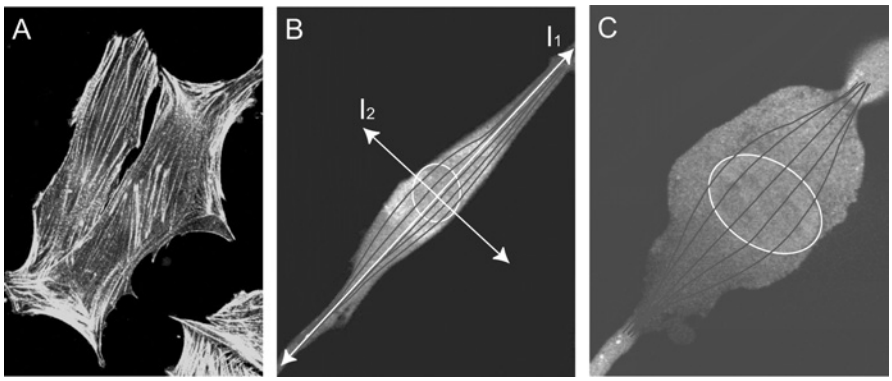

FIGURE 9. A: Actin fibers in two C2C12 cells. B,C: C2C12 cell with a schematic representation of the actin cytoskeleton, which is predominantly orientated along the first principal axis of the cell. As a result of the actin fibers, deformation of the cell and its nucleus is restricted in this direction.

deform mainly between the glass indenter and the cover glass.

At 45% axial deformation, a significant increase in cell volume was observed based on the nondeconvolved images. This increase might be the result of osmotic swelling due to malfunctioning pumps within the cell membrane. More likely, the volume increase can be attributed to the limited axial resolution of the confocal microscope, which is approximately 1.4 μm for the objective used in this study.[32,37] The limited axial resolution mainly affects the measurements of cell height and volume and will result in an overestimation of the two parameters, which was also observed in the measurements of the fluorescent beads (Appendix). Of course this effect will become more pronounced at large axial deformations. The use of deconvolution compensates to a certain extent for this limited axial resolution,[20,21] thereby reducing the overestimated height and volume of the cell. This can be observed in Fig. 7 in which the difference between the deconvolved and nondeconvolved data increased with axial deformation. Moreover, the volume increase based on the deconvolved images was never significantly different from zero. Another factor influencing the estimation of cell height and volume, is a mismatch in refractive index of the immersion medium (cell and growth medium) and the objective medium (air). To compensate for the resulting geometric distortion, a linear z-correction factor was introduced assuming a constant density. This assumption is valid for the measurements on homogeneous fluorescent beads, but not for cells. Therefore, future improvements on three-dimensional measurements of cell deformation will incorporate a z-correction factor depending on the location within the cell. This will require measurements of the refractive index distribution throughout the cell, which could be accomplished using optical coherence refractometry.[44]

The shape factor κ_{21} increased with axial compression, which was caused by a relative increase of I_2 (along the second principal axis) compared to I_1 (along the first principal axis). This can also be appreciated in Fig. 5, showing that the cell deforms more in the direction of the second principal axis than the first principal axis. Thus, the cell deforms in an anisotropic way. This anisotropic deformation may be attributed to actin stress fibers that form connections between the focal adhesion points at the substrate and the remainder of the cell body. Actin fibers largely contribute to the resistance against deformation of cells and disruption results in a decreased mechanical stiffness.[30,31] Visualization of actin fibers in fixed C2C12 cells stained with FITC-phalloidin revealed that they are predominantly orientated along the first principal axis of the cell [Fig. 9 (A)]. Because of the higher stiffness along the first principal axis as a result of the actin fibers, the cell deforms less in this direction [Figs. 9(B) and 9(C)]. If a cell does not have a preferred orientation of actin filaments, the deformation will probably be more or less isotropic. All cells examined in this study have a more or less elliptical shape and thus an orientated actin cytoskeleton. Notwithstanding these considerations, the importance of the actin cytoskeleton in determining anisotropic behavior could be further examined by compressing cells with and without actin stress fibers. At the same time, actin should be visualized during deformation of live cells using for example GFP-labelled (green fluorescent protein) actin.

It appears that this structural restriction to deformation is also applicable for the cell nucleus. Results suggest that the nucleus deformed more in the direction of the second principal axis than the first principal axis. This anisotropic deformation can be explained when considering a direct connection of the cytoskeleton to the nucleus [Figs. 9(B) and 9(C)]. Without this connection, the nucleus would deform isotropically as can be concluded from the nuclear structure, which shows no preferred fiber orientation.[33] Deformation of the nucleus during cell deformation has also been reported in chondrocytes in articular cartilage explants[15] and tenocytes in tendons.[2] Guilak[15] showed that the actin cytoskeleton plays an important role in the link between compression

of the extracellular matrix and deformation of chondrocyte nuclei. Furthermore, other studies report direct connections of the cell membrane to the nucleus via the cytoskeleton and address mechanical signalling to a cytoskeletal-mediated deformation of the nucleus.[3,4,19,38]

In summary, the deformation of attached myoblasts under compression was characterized using a single cell loading device in conjunction with confocal microscopy. A significant increase in surface area was found as a result of cell compression. No significant change in volume was found. It was shown that the cell and the nucleus deformed perpendicular to the direction of the actin filaments that run predominantly along the long axis of the cell. This strongly suggests that this anisotropic deformation can be attributed to the preferred orientation of actin filaments.

In future studies, the developed technique and loading device can be used to examine the relationship between cellular deformations and their biomechanical response, reflected by mechanical, structural, and functional changes. Furthermore, the methodology and results described here will be valuable to study strain-induced cell damage as seen in mechanically induced clinical conditions, such as pressure ulcers or repetitive strain injuries.

APPENDIX

To validate the image analysis method, the analysis was performed on mathematically defined shapes (cube and sphere) and images obtained from measurements on fluorescent beads with known diameter (FocalCheck, Molecular probes, the Netherlands) (Fig. A1). The mathematically defined cube had an edge length of 81 pixels and the sphere a diameter of 79 pixels. The fluorescent beads contain a green stain throughout and a red stain in a surface layer with a surface of less than 1 μm according to manufacturer specifications. For evaluation of the method, only the green stain of the bead was excited. To minimize refraction at the bead surface and thus prevent the relatively large bead acting as a lens, the beads were measured in immersion oil, which has almost the same refractive index as the fluorescent beads (1.52 compared to 1.56). A linear correction factor of 1.52 and a sampling density of $0.12 \times 0.12 \times 0.5$ μm^3 was used. The values of the geometric parameters of 10 beads and model geometric solids estimated by the above-mentioned method are listed in Tables A1 and A2. Furthermore, the percentage deviations of the measured values with the theoretical values are listed. The deviations for the fluorescent beads were calculated for each individual bead and subsequently averaged. The geometric parameters of the mathematical shapes were estimated within 4% deviation from the theoretical value, compared to 7% of the beads. An overestimation of approximately 6% of the height, volume, and surface area of the beads was observed. The estimates for the width and area of the beads were more accurate, resulting in an average percentage deviation of 2%. Using a Student's *t*-test with a 0.05 level of significance, it appeared that the mean values of the geometric parameters of the beads were never significantly different from the theoretically determined values.

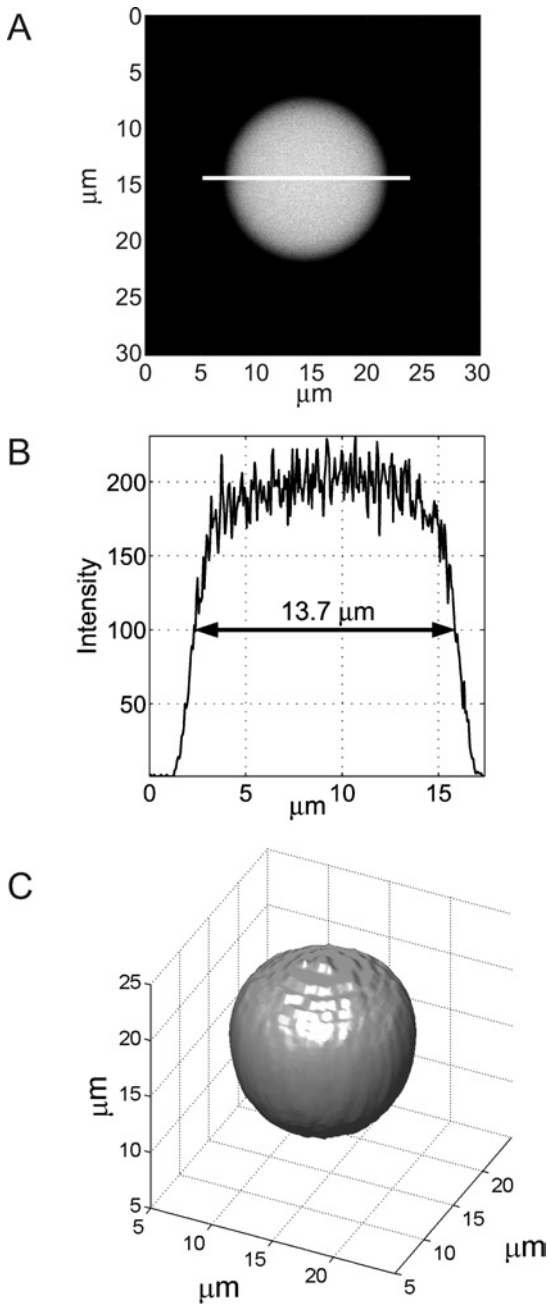

FIGURE A1. Confocal slice at the center of a fluorescent bead (A), the image intensity profile (B) obtained across the line in panel A and a three-dimensional reconstruction of the bead from all confocal slices (C). The full width half maximum threshold resulted in a measured width of 13.7 μm.

TABLE A1. Estimated (e) and theoretical (t) values of the width (W in μm), height (H in μm), and cross-sectional area (A in μm^2) of the model geometric solids and fluorescent beads ($n = 10$) (mean ± SD).

Object	W_e	W_t	%	H_e	H_t	%	A_e	A_t	%
Cube	81	81	0	81	81	0	6561	6561	0
Sphere	79	79	0	79	79	0	4984	5026	−0.8
Bead	13.7 ± 0.2	14	−2 ± 1	14.6 ± 0.3	14	4.2 ± 2.3	151 ± 3	154	−1.8 ± 1.8

TABLE A2. Estimated (e) and theoretical (t) values of the surface area (SA in μm^2) and volume (V in μm^3) of the model geometric solids and fluorescent beads ($n = 10$) (mean ± SD).

Object	SA_e	SA_t	%	V_e	V_t	%
Cube	38025	39366	−3.4	531441	531441	0
Sphere	19874	19607	1.4	264712	258150	2.5
Bead	656 ± 28	616	6.4 ± 4.6	1528 ± 59	1437	6.3 ± 4.1

ACKNOWLEDGMENTS

The authors thank Roel Janssen for his contribution to the measurements on the fluorescent beads and deconvolution.

REFERENCES

[1] Alcaraz, J., L. Buscemi, M. Grabulosa, X. Trepat, B. Fabry, R. Farre, and D. Narajas. Microrheology of human lung epithelial cells measured by atomic force microscopy. *Biophys. J.* 84:2071–2079, 2003.

[2] Arnoczky, S. P., M. Lavagnino, J. H. Whallon, and A. Hoonjan. *In situ* cell nucleus deformation in tendons under tensile load: A morphological analysis using confocal laser microscopy. *J. Orthop. Res.* 20:29–35, 2002.

[3] Banes, A. J., M. Tsuzaki, P. Hu, B. Brigman, T. Brown, and L. Miller. Mechanoreception at the cellular level: The detection, interpretation, and diversity of responses to mechanical signals. *Biochem. Cell Biol.* 73:349–365, 1995.

[4] Ben-Ze'ev, A. Animal cell shape changes and gene expression. *Bioessays* 13:207–212, 1991.

[5] Bhadriraju, K., and L. K. Hansen. Extracellular matrix- and cytoskeleton-dependent changes in cell shape and stiffness. *Exp. Cell Res.* 278:92–100, 2002.

[6] Bouten, C. V. C., M. M. Knight, D. A. Lee, and D. L. Bader. Compressive deformation and damage of muscle cell subpopulations in a model system. *Ann. Biomed. Eng.* 29:153–163, 2001.

[7] Brodland, G. W., and J. H. Veldhuis. Computer simulations of mitosis and interdependencies between mitosis orientation, cell shape and epithelia reshaping. *J. Biomech.* 35:673–681, 2002.

[8] Bucher, D., M. Scholz, M. Stetter, K. Obermayer, and H. J. Pflüger. Correction methods for three-dimensional reconstructions from confocal images: I. Tissue shrinking and axial scaling. *J. Neurosci.* 100:135–143, 2000.

[9] Caille, N., O. Thoumine, Y. Tardy, and J.-J. Meister. Contribution of the nucleus to the mechanical properties of endothelial cells. *J. Biomech.* 35:177–187, 2002.

[10] Chen, C. S., M. Mrksich, S. Huang, G. M. Whitesides, and D. E. Ingber. Geometric control of cell life and death. *Science* 276:1425–1428, 1997.

[11] Coughlin, M. F., and D. Stamenović. A tensegrity model of the cytoskeleton in spread and round cells. *J. Biomech. Eng.* 120:770–777, 1998.

[12] Daily, B., and E. L. Elson. Cell poking: Determination of the elastic area compressibility modulus of the erythrocyte membrane. *Biophys. J.* 45:671–682, 1984.

[13] Errington, R. J., M. D. Fricker, J. L. Wood, A. C. Hall, and N. S. White. Four-dimensional imaging of living chondrocytes in cartilage using confocal microscopy: A pragmatic approach. *Am. J. Physiol.* 272:104–1051, 1997.

[14] Evans, E., and A. Yeung. Apparent viscosity and cortical tension of blood granulolcytes determined by micropipet aspiration. *Biophys. J.* 56:151–160, 1989.

[15] Guilak, F. Compression-induced changes in the shape and volume of the chondrocyte nucleus. *J. Biomech.* 28:1529–1541, 1995.

[16] Guilak, F., A. Ratcliffe, and C. Mow. Chondrocyte deformation and local tissue strain in articular cartilage: A confocal microscopy study. *J. Orthop. Res.* 13:410–421, 1995.

[17] Hell, S., G. Reiner, C. Cremer, and E. H. K. Stelzer. Aberrations in confocal fluorescence microscopy induced by mismatches in refractive index. *J. Microsc.* 169:391–405, 1993.

[18] Ingber, D. E. Cellular tensegrity: Defining new rules of biological design that govern the cytoskeleton. *J. Cell Sci.* 104:613–627, 1993.

[19] Janmey, P. A. The cytoskeleton and cell signaling: Component localization and mechanical coupling. *Physiol. Rev.* 78:763–781, 1998.

[20] Kano, H., H. T. M. Voort, M. Schrader, G. M. P. Kempen, and S. W. Hell. Avalanche photodiode detection with object scanning and image restoration provides 2–4 fold resolution increase in two-photon fluorescence microscopy. *Bioimaging* 4:187–197, 1996.

[21] Kempen, G. M. P., L. J. van Vliet, P. J. Verveer, and H. T. M. van der Voort. A quantitative comparison of image restoration methods for confocal microscopy. *J. Microsc.* 185:354–365, 1997.

[22] Knight, M. M., D. A. Lee, and D. L. Bader. Distribution of chondrocyte deformation in compressed agarose gel using confocal microscopy. *Med. Biol. Eng. Comput.* 1:97–102, 1996.

[23] Koay, E. J., A. C. Shieh, and K. A. Athanasiou. Creep indentation of single cells. *J. Biomech. Eng.* 125:334–341, 2003.

[24] Lee, D. A., M. M. Knight, J. F. Bolton, B. D. Idowu, M. V. Kayser, and D. L. Bader. Chondrocyte deformation within

compressed agarose constructs at the cellular and sub-cellular levels. *J. Biomech.* 33:81–95, 2000.

[25]Maniotis, A. J., C. S. Chien, and D. E. Ingber. Demonstration of mechanical connections between integrins, cytoskeletal filaments, and nucleoplasm that stabilize nuclear structure. *Proc. Natl. Acad. Sci. U.S.A.* 94:849–854, 1997.

[26]McConnaughey, W. B., and N. O. Petersen. The cell poker: An apparatus for stress-strain measurements on living cells. *Rev. Sci. Instrum.* 51:575–580, 1980.

[27]Mooney, D., L. Hansen, J. Vacanti, R. Langer, S. Farmer, and D. Ingber. Switching from differentiation to growth in hepatocytes: Control by extracellular matrix. *J. Cell. Physiol.* 151:497–505, 1992.

[28]Needham, D., and R. M. Hochmuth. Rapid flow of passive neutrophils into a 4 μm pipet and measurement of cytoplasmic viscosity. *J. Biomech. Eng.* 112:269–276, 1990.

[29]Peeters, E. A. G., C. V. C. Bouten, C. W. J. Oomens, and F. P. T. Baaijens. Monitoring the biomechanical response of individual cells under compression: A new compression device. *Med. Biol. Eng. Comput.* 41:498–503, 2003.

[30]Petersen, N. O., W. B. McConnaughey, and E. L. Elson. Dependence of locally measured cellular deformability on position on the cell, temperature, and cytochalalasin B. *Proc. Natl. Acad. Sci. U.S.A.* 79:5327–5331, 1982.

[31]Sato, M., D. P. Theret, L. T. Wheeler, N. Ohshima, and R. M. Nerem. Application of the micropipette technique to the measurement of cultured porcine aortic endothelial cell viscoelastic properties. *J. Biomech. Eng.* 112:263–268, 1990.

[32]Sheppard, J. Axial resolution of confocal fluorescence microscopy. *J. Microsc.* 154:237–241, 1989.

[33]Stuurman, N., S. Heins, and U. Aebi. Nuclear lamins: Their structure, assembly and interactions. *J. Struct. Biol.* 122:42–66, 1998.

[34]Thoumine, O., and O. Cardoso. Changes in the mechanical properties of fibroblasts during spreading: A micromanimpulation study. *Eur. Biophys. J.* 28:222–234, 1999.

[35]Thoumine, O., A. Ott, O. Cardoso, and J. Meister. Microplates: A new tool for manipulation and mechanical perturbation of individual cells. *J. Biochem. Biophys. Methods* 39:47–62, 1999.

[36]Vesenka, J., C. Mosher, S. Schaus, L. Ambrosio, and E. Henderson. Combining optical and atomic force microscopy for life sciences research. *Biotechniques* 19:240–253, 1995.

[37]Visser, T. D., J. L. Oud, and G. J. Brakenhoff. Refractive index and axial distance measurements in 3D microscopy. *Optik* 90:17–19, 1992.

[38]Wang, N., J. P. Butler, and D. E. Ingber. Mechanotransduction across the cell surface and through the cytoskeleton. *Science* 260:1124–1127, 1993.

[39]Wang, N., and D. E. Ingber. Control of cytoskeletal mechanics by extracellular matrix, cell shape and mechanical tension. *Biophys. J.* 66:2181–2189, 1994.

[40]Watson, P. A. Function follows form: Generation of intracellular signals by cell deformation. *FASEB J.* 5:2013–2019, 1991.

[41]Wilson, T. Optical sectioning in confocal fluorescent microscopes. *J. Microsc.* 154:143–156, 1989.

[42]You, H. X., J. M. Lau, S. Zhang, and L. Yu. Atomic force microscopy imaging of living cells: A preliminary study of the disruptive effect of the cantilever tip on cell morphology. *Ultramicroscopy* 82:297–305, 2000.

[43]Zhang, Z., M. A. Ferenczi, A. C. Lush, and C. R. Thomas. A novel micromanipulation technique for measuring the bursting strength of single mammalian cells. *Appl. Microbiol. Biotechnol.* 36:208–210, 1991.

[44]Zvyagin, A. V., K. K. M. B. D. Silva, S. A. Alexandrov, T. R. Hillman, J. J. Armstrong, T. Tsuzuki, and D. D. Sampson. Refractive index tomography of turbid media by bifocal optical coherence refractometry. *Opt. Express* 11:3503–3517, 2003.